Nanoscale

PAPER

View Article Online
View Journal | View Issue

Cite this: *Nanoscale*, 2015, **7**, 14047

The patterning mechanism of carbon nanotubes using surface acoustic waves: the acoustic radiation effect or the dielectrophoretic effect†

Zhichao Ma,[a] Jinhong Guo,[a] Yan Jun Liu[b] and Ye Ai*[a]

Received 26th June 2015,
Accepted 16th July 2015

DOI: 10.1039/c5nr04272k

www.rsc.org/nanoscale

In this study, we present a simple technique capable of assembling and patterning suspended CNTs using a standing surface acoustic wave (SSAW) field. Individual CNTs could be assembled into larger CNT bundles and patterned in periodic positions on a substrate surface. The mechanism of the SSAW-based patterning technique has been investigated using both numerical simulation and experimental study. It has been found that the acoustic radiation effect due to the acoustic pressure field and the dielectrophoretic (DEP) effect induced by the electric field co-existing in the patterning process however play different roles depending on the properties of the suspended particles and the suspension medium. In the SSAW-based patterning of highly conductive CNTs with high aspect ratio geometry, the positive DEP effect dominates over the acoustic radiation effect. In contrast, the acoustic radiation effect dominates over the DEP effect when manipulating less conductive, spherical or low aspect ratio particles or biological cells. These results provide a meaningful insight into the mechanism of SSAW-based patterning, which is of great help to guide the effective use of this patterning technique for various applications.

1. Introduction

Since the discovery of carbon nanotubes (CNTs),[1] their distinctive electrical, thermal and mechanical properties[2–5] have led to various applications in material engineering, microelectronics, energy storage and biotechnology.[6] Patterning and assembling of CNTs has been a vital technique to facilitate applications of CNTs in chemical sensors,[7–9] transistors[10,11] and flexible supercapacitors.[12,13] There are mainly two types of techniques to achieve this goal: direct growth of CNTs on certain substrates with pre-patterned nanostructures[14] and positioning of randomly suspended CNTs onto substrates. The latter typically benefit from a relatively simple and cost effective process compared to the direct growth approach. To date, various strategies for precise positioning of CNTs such as chemical assembling,[15] contact printing,[16] spin-coating assistance[17] and dielectrophoresis[18] have been reported. However, each of these methods has its own limitations. For example, chemical and spin-coating assisted assembly of CNTs involves a complex chemical treatment process; the contact printing method does not offer alignment for CNTs; current dielectrophoresis-based patterning is controlled by fixed arrangements of pre-fabricated microelectrodes and thus lacks flexibility.

In recent years, standing surface acoustic waves (SSAW) have emerged as a promising non-contact technique for manipulating synthetic micron-sized particles and biological cells in suspension.[19–24] This technique makes use of the acoustic radiation effect by the standing field to move suspended particles to specific locations, which is ideal for precise patterning in the microscale regime. For example, the SSAW-based manipulation technique has been used to assemble biological cells in tunable 1D patterns[25] or 2D patterns[26] for cell–cell interaction studies.[27,28] Most recently, the SSAW-based technique has also been successfully demonstrated to pattern rod-shaped nanowires[29] and CNTs.[30,31] In all the reported studies related to cell patterning, the acoustic radiation force acting on suspended cells is considered as the dominant effect. In contrast, the aforementioned studies related to the patterning of rod-shaped nanoparticles attribute the dominant effect to the dielectrophoretic (DEP) force generated by the alternating current (AC) electrical field in the suspension. It is worth mentioning that the patterning of cells and nanoparticles uses a similar configuration to generate the SSAW field in the suspension. In addition, the acoustic radiation force and DEP force are both linearly proportional to the particle size, which implies that the size effect is not determin-

[a]Pillar of Engineering Product Development, Singapore University of Technology and Design, Singapore 487372, Singapore. E-mail: aiye@sutd.edu.sg; Tel: (+65) 6499 4553
[b]Institute of Materials Research and Engineering, Agency for Science Technology and Research (A*STAR), Singapore 117602, Singapore

†Electronic supplementary information (ESI) available. See DOI: 10.1039/c5nr04272k

ing the dominance of the two effects. Therefore, the two forces may co-exist in the SSAW-based patterning process. However, the contribution of the two forces in different patterning schemes has not been carefully investigated until now.

In this study, we present an SSAW-based CNT patterning approach, which offers a suspension-based strategy for large-scale and affordable patterning of CNTs. Scanning electron microscopy (SEM) offers details of how CNTs are assembled and patterned into even larger bundles. Transferring of patterned CNTs from piezoelectric substrates onto polymer materials has been realized, which ensures this method as a promising patterning technique to be further exploited for practical applications. In particular, both experimentation and simulation have been conducted to investigate the mechanism of CNT patterning using the SSAW field. The roles of the acoustic radiation force and the DEP force in the CNT patterning have been clearly explained, which provides a meaningful insight into this non-contact patterning technique.

2. Methods

2.1 Experimental setup

Fig. 1a shows the schematic illustration of the microfluidic device for SSAW-based patterning. Two interdigital transducers (IDTs) for SAW generation were fabricated by depositing micro-electrodes onto a 128° rotated Y-cut X-propagating lithium niobate ($LiNbO_3$) piezoelectric substrate with a lift-off technique.[20] Briefly, double metallic layers (Cr/Au) were deposited onto a pre-patterned photoresist on the $LiNbO_3$ substrate by using an electron beam evaporator. The undesired metallic region was washed away together with the photoresist with acetone with the assistance of sonication. Each IDT has 20 electrode finger pairs with 75 μm width and 75 μm space. The aperture of the two IDTs is 12 mm and the distance between the two IDTs is 10 mm. The resonance frequency was found around 13.1 MHz. A microchamber was placed in the midst of the two IDTs for loading the CNT suspensions. It was made of polydimethylsiloxane (PDMS) using a widely known soft lithography technique. The microchamber has a height of 50 μm and an area of 6 × 6 mm^2. After the microchamber was brought into contact with the $LiNbO_3$ substrate to form the microfluidic device, 0.1 wt% deionized water based metallic multi-walled carbon nanotube (MWCNT) suspension was introduced by capillary force into the microchamber, sandwiched between the PDMS layer and the $LiNbO_3$ substrate.

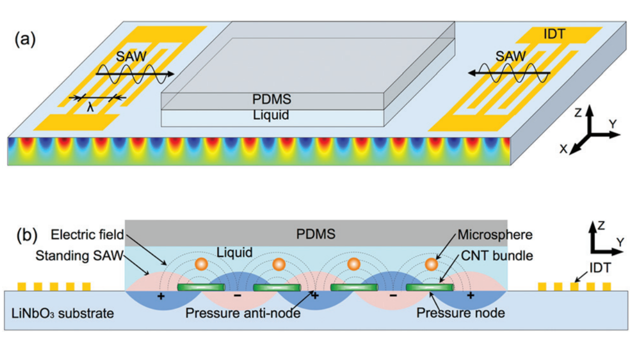

Fig. 1 (a) Schematic illustration of the experimental setup for SSAW-based patterning. A PDMS microchamber for suspension loading is placed in the midst of two pairs of IDTs on the $LiNbO_3$ substrate. (b) Cross-sectional view of the patterning of two types of suspended particles. SSAW field and electric field co-exist in the suspension, which exert the acoustic radiation force and the DEP force on suspended particles, respectively.

An AC sinusoidal signal at the resonance frequency, generated by a signal generator, was amplified using a power amplifier and then split into two identical signals to drive the two IDTs. Upon excitation by the AC signal, the IDT converts the electric field into acoustic waves, which is basically a mechanical vibration on the surface of the $LiNbO_3$ substrate. Two identical travelling SAWs propagate toward the chamber in opposite directions, which in turn gives rise to a SSAW field arising from the constructive interference of the two waves. The mechanical vibration in the chamber region accordingly generates an electric field due to the piezoelectric effect, which is schematically illustrated in Fig. 1b. Therefore, the SSAW field and the electric field co-exist in the suspension, which exert the acoustic radiation force and the DEP force on suspended particles, respectively. The patterning process was monitored under a CCD camera equipped on an inverted optical microscope. Patterned CNTs were further examined using SEM.

2.2 Numerical model

A numerical model developed in our previous study[32] was applied to examine the SSAW field and the electric field in the suspension. Generally, this numerical model solves linear piezoelectric constitutive equations, consisting of the Maxwell's equations for electric field and the stress–strain equations for mechanical motion. Once the acoustic pressure field in the suspension is determined, the time-averaged acoustic radiation force acting on suspended particles can be expressed as[33]

$$\langle F_{\mathrm{aco}}\rangle = -\nabla\left\{\frac{V_{\mathrm{p}}}{4\rho_{\mathrm{m}}{c_{\mathrm{m}}}^2}\left[2\left(1-\frac{1}{\beta\gamma^2}\right)\langle p^2\rangle - \frac{2\beta-2}{2\beta+1}\frac{3}{n^2}\langle|\nabla p|^2\rangle\right]\right\}, \tag{1}$$

where V_p is the volume of the particle, ρ_m and c_m are the density and sound speed of the suspension medium, respectively. β and γ is the density ratio and the sound speed ratio of the particle to the suspension medium, respectively. p is the acoustic pressure generated by the SSAW field, $n = 2\pi/\lambda$ is the wavenumber with λ being the SAW wavelength.

In most existing studies on the SSAW-based patterning, the acoustic pressure field is approximated as a one-dimensional distribution across the microfluidic channel or chamber, which further simplifies eqn (1), given as[34]

$$\langle F_{\mathrm{aco}}\rangle = \frac{nV_{\mathrm{p}}{p_0}^2}{4\rho_{\mathrm{m}}{c_{\mathrm{m}}}^2}\varphi(\beta,\gamma)\sin(2nx), \tag{2}$$

where x is the distance from the pressure node, and the acoustic contrast factor that can determine the force direction is given as

$$\varphi(\beta,\gamma) = \frac{5\beta - 2}{2\beta + 1} - \frac{1}{\beta\gamma^2}. \quad (3)$$

A SSAW field provides a series of pressure nodes and antinodes with a space of half the wavelength. Solid particles suspended in aqueous medium generally have a positive acoustic contrast factor, and are typically pushed towards the pressure nodes.

When a polarizable particle is suspended in an inhomogeneous electric field, it will be polarized and experience the DEP force.[35,36] In an AC electric field, the time-averaged DEP force acting on a particle is expressed as[37–39]

$$\langle F_{\mathrm{dep}} \rangle = G_{\mathrm{a}} V_{\mathrm{p}} \varepsilon_{\mathrm{m}} \mathrm{Re}\{f_{\mathrm{cm}}(\omega)\} \nabla |E_{\mathrm{rms}}|^2, \quad (4)$$

where G_a is the factor dependent on the particle geometry, ε_m is the real part of the permittivity of the suspension medium, and E_{rms} is the root mean square value of the electric field. The direction of the DEP force is dependent on the real part of the Clausius–Mossotti factor, $\mathrm{Re}\{f_{cm}(\omega)\}$. When $\mathrm{Re}[f_{cm}(\omega)] > 0$, *i.e.* the particle is more polarizable than the suspension medium, the DEP force pushes the particle toward the region with a maximum electric field, typically moving toward the electrodes. This phenomenon is known as positive DEP. Oppositely, while $\mathrm{Re}[f_{cm}(\omega)] < 0$, the DEP force repels the particles toward the region with a minimum electric field, typically moving away from the electrodes, which is known as negative DEP.

3. Results and discussion

3.1 Patterning CNTs in suspension

After introduction into the chamber, the CNT suspension formed a 50 μm thick static film and CNTs were uniformly dispersed in the suspension without observed aggregation, as shown in Fig. 2a. Subsequently, a 30 V_{pp} AC sinusoidal signal was immediately applied on the two IDTs. Within 5 seconds, parallel lines of assembled CNT bundles in the suspension were observed, as shown in Fig. 2b and c at different magnifications (Video 1 in the ESI†). These patterned parallel lines were perpendicular to the direction of the SAW propagation. The pitch between each line was around 150 ± 6 μm, which approaches half the wavelength of the SSAW field. The width of each assembling line was around 67 ± 3 μm. Individual CNT bundles in all the assembling lines were however parallel to the direction of the SAW propagation. As a result of heating and atomization by SAW, the water in the suspension evaporates in 150–200 s, which was much faster than that in the absence of the SSAW field. During the aqueous medium evaporation, the CNT patterns were well retained without damage or disturbance.

After the suspension medium evaporation, the CNT patterns were transferred onto PDMS for SEM observation. Liquid PDMS was poured on the substrate and then baked at 70 °C for 20 minutes. Subsequently, the cured PDMS was peeled off from the substrate and the CNT patterns were transferred onto the PDMS layer with high fidelity (Fig. S1 in the ESI†). Although the pattern transfer in this study is mainly for the convenience of SEM observation, the high fidelity transferring of CNT patterns onto other polymer materials demonstrates that it has great potential in assembling and patterning CNTs for various sensing applications such as flow sensors,[40] body motion sensors[41–43] and flexible supercapacitors.[12]

Fig. 3 shows the SEM photographs of both unpatterned (Fig. 3a–c) and patterned (Fig. 3d–f) CNTs transferred onto the PDMS. The unpatterned CNTs refer to a random distribution of CNTs on the substrate, which were obtained by naturally evaporating the CNT suspension in the chamber without applying the SSAW field. After actuating the CNT suspension by a SSAW field, CNTs were assembled into much longer CNT bundles aligned with the SSAW field (Fig. 3d–f).

3.2 Patterning mechanism

A few previous studies[29–31] attribute the SSAW-based patterning of conductive nanowires and CNTs to the dominant DEP effect generated by an alternating electric potential distribution along the piezoelectric substrate. However, all the

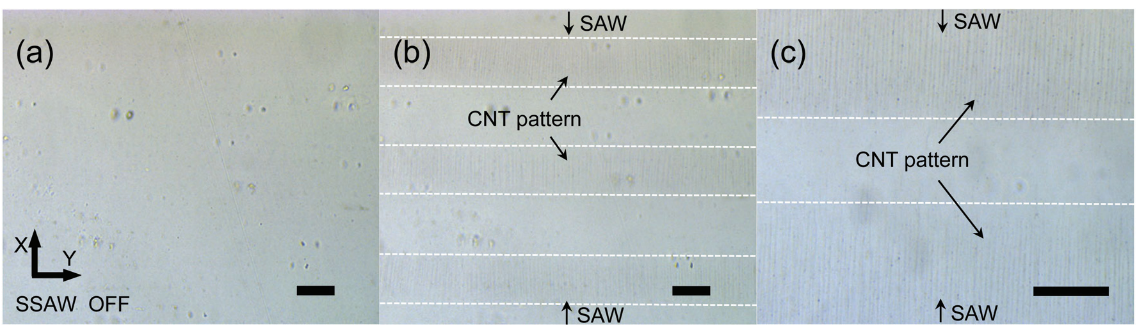

Fig. 2 Patterning of CNTs using a SSAW field. CNTs well dispersed in the suspension medium without aggregation before applying the SSAW field (a). Periodic CNT patterns formed after applying the SSAW field (b: 20× and c: 40×). The scale bars are all 50 μm.

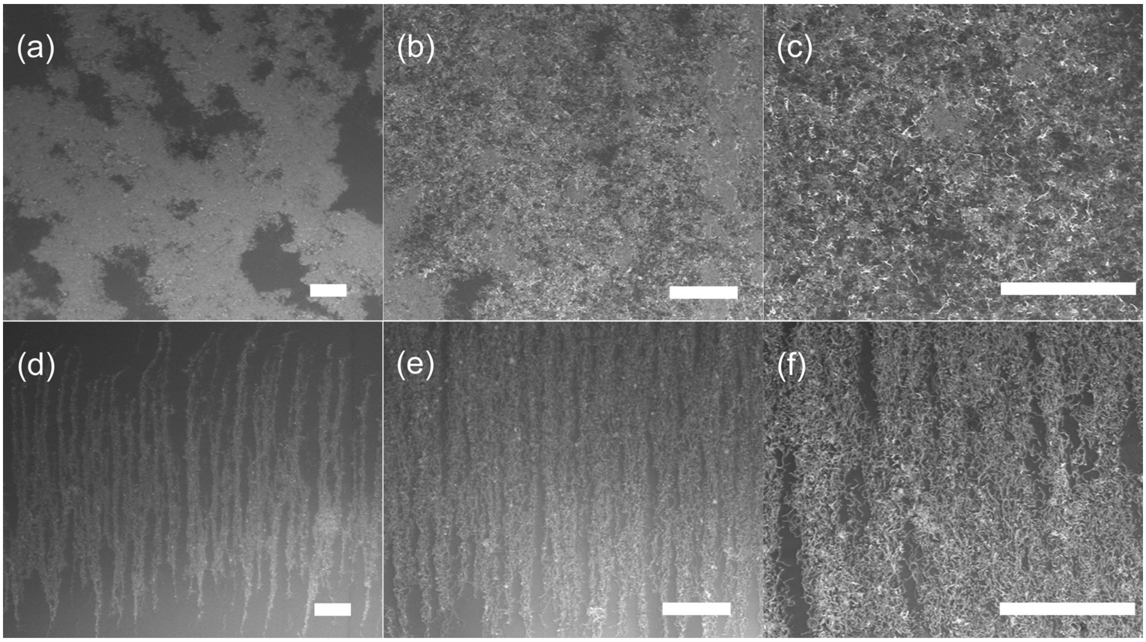

Fig. 3 SEM photographs of unpatterned (a–c) and patterned (d–f) CNT bundles transferred onto PDMS at different magnifications (800×, 1500×, 3000× from left to right). The scale bars are all 10 μm.

studies related to the patterning of biological cells claim that acoustophoresis arising from the acoustic radiation effect is responsible for the cell motion subjected to a SSAW field. The two forces may co-exist in the SSAW-based patterning of suspended particles in the suspension. However, their roles and contribution have not been well investigated by far. This section aims to clearly explain the patterning mechanism under a SSAW field.

Fig. 4a shows the simulated acoustic pressure of a SSAW field in a 50 μm thick liquid layer, which is generated by the interference of two identical counter-propagating SAWs. Periodic distribution of pressure nodes along the horizontal direction of the liquid layer is predicted. The acoustic contrast factor of CNT is 1.426, referring to a positive acoustophoresis (the properties of patterned particles are listed in Table S1 in the ESI†). Therefore, the acoustic radiation effect tends to push suspended particles toward the pressure nodes where the acoustic pressure magnitude is zero. The propagating mechanical vibration of the piezoelectric substrate accordingly generates a periodic distribution of electric potential along the substrate surface, acting as virtual electrodes in contact with the liquid layer (Fig. 4b). The interfaces between opposite polarities refer to the potential nodes. As a result, a periodic electric field with the same wavelength and frequency is also present in the liquid layer and thus give rise to the DEP-induced particle motion. It is found that the pressure nodes and potential nodes are generated in the same periodic positions.

Once the acoustic pressure field and electric field are simulated, the acoustic radiation force and DEP force can be determined using eqn (1) and (4), respectively. Here, we consider a single CNT with a length of 1 μm and a diameter of 40 nm. Fig. 4c shows the distribution of the acoustic radiation force along the horizontal direction, which dominates the acoustophoresis of suspended particles to the pressure nodes. The maximum magnitude is around 0.4 fN. To determine the DEP force acting on a single CNT, we approximate the CNT as a long prolate spheroid. Therefore, the real part of the Clausius–Mossotti factor is calculated as[44]

$$f_{\mathrm{cm}}(\omega)=\frac{\varepsilon_{\mathrm{p}}^{*}-\varepsilon_{\mathrm{m}}^{*}}{\left(\varepsilon_{\mathrm{p}}^{*}-\varepsilon_{\mathrm{m}}^{*}\right)A_{\alpha}+\varepsilon_{\mathrm{m}}^{*}},\quad \varepsilon^{*}=\varepsilon-j\frac{\sigma}{\omega},\tag{5}$$

$$A_{\alpha}=-\frac{b^{2}}{2a^{2}e^{3}}\left(2e-\ln\frac{1+e}{1-e}\right),\quad e=\sqrt{1-\frac{b^{2}}{a^{2}}},\tag{6}$$

where $\varepsilon_{\mathrm{p}}^{*}$ and $\varepsilon_{\mathrm{m}}^{*}$ are the complex permittivities of the particle and the suspension medium. ε is the permittivity, σ is conductivity, $\omega = 2\pi f$ is the angular frequency of the electric field, and $\mathrm{j}=\sqrt{-1}$ is the imaginary unit. a and b are the equatorial radius and polar radius of the approximated prolate spheroid, respectively. Therefore, the CNT length is $2a$ and the CNT diameter is $2b$. In this case, $a/b = 25$ and thus the calculated real part of the Clausius–Mossotti factor is 214. Accordingly, CNTs experience positive DEP and tend to move toward the region with a higher electric field. Fig. 4d shows the DEP force along the horizontal direction, which tends to push CNTs towards the potential nodes. Therefore, the acoustic radiation force and DEP force concentrate suspended CNTs to the same periodic positions horizontally. The maximum magnitude of the horizontal DEP force is beyond 2 fN, which is 5 times higher than the acoustic radiation force. Fig. 4e shows that the verti-

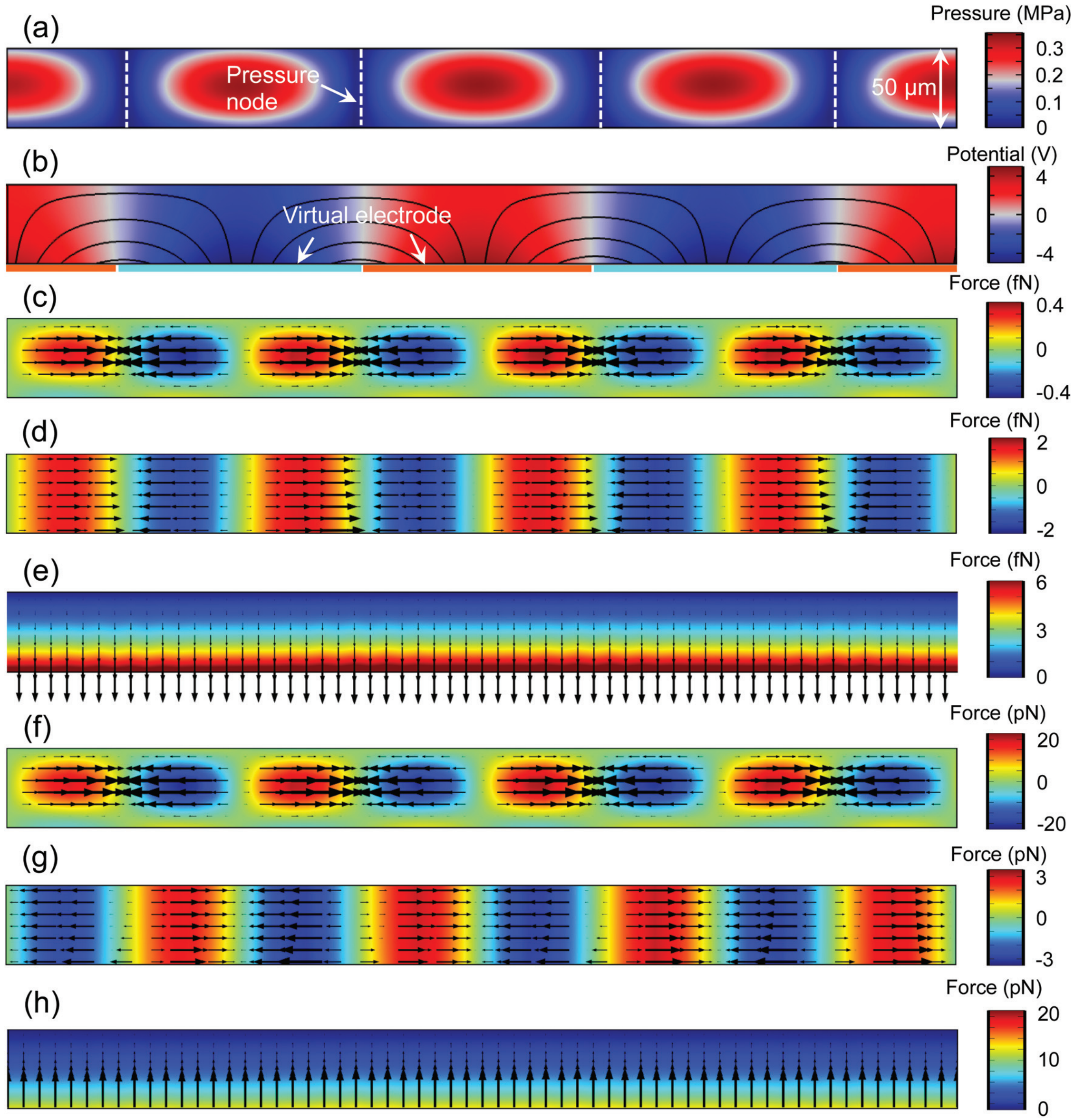

Fig. 4 Numerical simulation results. Acoustic pressure field (a) and electric field (b) in a 50 μm thick suspension. Dashed lines in (a) represent the periodic positions of the pressure nodes. The alternating potential distribution along the piezoelectric substrate is considered as periodic virtual electrodes in (b). Horizontal acoustic radiation forces acting on CNTs (c) and polystyrene particles (f) push them towards the pressure nodes. Horizontal DEP forces acting on CNTs (d) and polystyrene particles (g) push the CNTs and the particles towards the pressure nodes and the pressure anti-nodes, respectively. Vertical DEP force attracts CNTs to the substrate surface (e); while pushes polystyrene particles away from the substrate surface (h).

cal DEP force tends to attract CNTs onto the substrate surface. The maximum magnitude of the vertical DEP force is more than 3 times higher than that of the horizontal DEP force. When $a/b = 50$, the real part of the Clausius–Mossotti factor is 693. In such case, the DEP force would be more than 50 times higher than the acoustic radiation force. Therefore, the positive DEP effect dominates over the acoustic radiation effect in the patterning of CNTs. In particular, the DEP force is able to assemble individual CNTs into much larger CNT bundles oriented parallel with respect to the electric field.[45,46] Based on the simulation result, it is predicted that the assembled CNT bundles are patterned to the potential nodes (also the pressure nodes) on the substrate surface due to the dominant positive DEP effect.

Next, we use the same numerical model to simulate the acoustic radiation force and DEP force acting on polystyrene particles with a diameter of 6 μm. Note that polystyrene particles are subjected to the same acoustic pressure field and electric field as the CNT suspension. The acoustic contrast factor of polystyrene particles is 0.669, implying that acoustophoresis tends to move these particles toward the pressure nodes. Fig. 4f shows the distribution of the horizontal acoustic

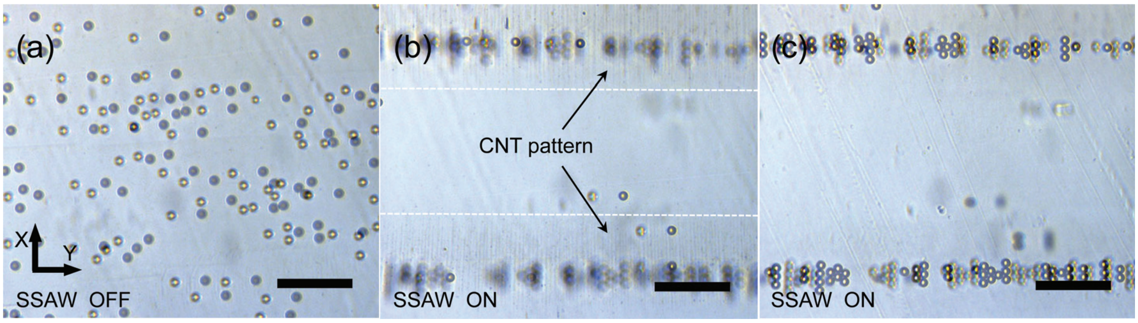

Fig. 5 Patterning of a mixture including CNTs and polystyrene particles. Well-dispersed suspension before applying the SSAW field (a). Microscopic photographs on different focal planes with clear images of CNT patterns (b) and microsphere patterns (c) after applying the SSAW field. The scale bars are all 50 μm.

radiation force with a maximum magnitude around 20 pN. The real part of the Clausius–Mossotti factor of a spherical particle is calculated as[44]

$$f_{\mathrm{cm}}(\omega) = \frac{\varepsilon_{\mathrm{p}}^{*} - \varepsilon_{\mathrm{m}}^{*}}{\varepsilon_{\mathrm{p}}^{*} + 2\varepsilon_{\mathrm{m}}^{*}}, \tag{7}$$

which is −0.476 for spherical polystyrene particles. Therefore, polystyrene particles experience negative DEP that moves particles toward the region with a lower electric field. As a result, the horizontal DEP force is in the opposite direction of the acoustic radiation force (Fig. 4g). In other words, the acoustic radiation force pushes particles towards the pressure nodes; while the negative DEP force pushes particles towards the pressure anti-nodes. However, the maximum magnitude of the horizontal DEP force is around 3 pN, which is much smaller than the acoustic radiation force. Therefore, the acoustic radiation effect dominates over the DEP effect in the patterning of spherical polystyrene particles. The significant decrease in the real part of the Clausius–Mossotti factor is mainly responsible for the minor DEP effect in this case. When the suspended particles are more conductive than the medium, a rod-shaped particle typically has a higher real part of the Clausius–Mossotti factor than a spherical particle, which is also confirmed in a previous study.[44] Therefore, a rod-shaped particle may experience a much stronger DEP force than a spherical particle with an equivalent volume. The shape-dependent DEP effect explains why positive DEP force is the dominant effect in the patterning of highly conductive CNTs with high aspect ratio geometry and acoustophoresis is the dominant effect in the patterning of less conductive particles and biological cells with low aspect ratio geometry. Fig. 4h shows that the vertical component of the negative DEP force tends to repel CNTs away from the substrate surface. The magnitude of the vertical DEP force also decays rapidly from the substrate surface. Based on this simulation, it is predicted that polystyrene particles are also patterned on the pressure nodes (potential nodes) due to the dominant acoustic radiation effect and they suspend away from the substrate surface due to the repulsive DEP force in the vertical direction.

To validate our hypothesis on the basis of the numerical simulation, the patterning of a mixed suspension containing both CNTs and 6 μm polystyrene microspheres (Fig. 5a) was performed. Once the SSAW field was generated across the chamber, as shown in Fig. 5b and c, the microspheres and CNTs were patterned in the same horizontal positions, which was in good agreement with the numerical simulation. These patterning positions should be the periodic pressure nodes, which are the potential nodes of the electric field as well. Note that Fig. 5b and c show the focal planes with clear images of CNT pattern and microsphere pattern, respectively. The misfocusing of the two patterns reveals that CNTs and microspheres were concentrated at different heights. In particular, during the evaporation process, the assembled and patterned CNT bundles were well retained without damage or disturbance; however, the patterned microspheres were washed away by the movement of the evaporating liquid layer (Video 2 in the ESI†). This experimental observation confirms that the CNTs were attracted on the substrate surface so their pattern could not be affected by the liquid evaporation. In contrast, the patterned microspheres were suspended above the substrate surface and thus were sensitive to the liquid motion. As explained previously by the numerical simulation, CNTs experienced a positive DEP force and were accordingly attached on the substrate surface; while the microspheres experienced a negative DEP force and were thus repelled away from the substrate surface. These experimental results verify the mechanism analysis of the SSAW-based patterning technique.

4. Conclusions

Aqueous suspension-based CNT assembly on the cm^2 scale has been achieved using a SSAW field. Individual CNTs could be assembled into larger CNT bundles that are oriented parallel with respect to the direction of the SAW propagation. The space between the adjacent CNT patterns is half the SAW wavelength. The acoustic pressure field and the electric field coexist in the aqueous suspension, which accordingly induce the acoustic radiation effect and the DEP effect that may both affect the patterning process. Numerical simulation and experimentation have been used to investigate the mechanism of SSAW-based particle patterning. It has been found that the positive DEP effect dominates over the acoustic radiation effect in the patterning of CNTs. This unique phenomenon is attributed to the fact that the highly conductive CNTs with high aspect ratio geometry have a much higher real part of the Clausius–Mossotti factor than polymer microspheres or biological cells (typically from a few hundreds to tens of hundreds higher). Because of the dominant positive DEP effect, CNTs are patterned in periodic positions (potential nodes) on the substrate surface, and can be well retained during the liquid evaporation process. In contrast, the acoustic radiation effect dominates over the DEP effect in the patterning of spherical or low aspect ratio and less conductive particles, which is more common in the cell manipulation using SSAW fields. The high fidelity transferring of CNT patterns onto PDMS demonstrates its potential in assembling and patterning CNTs for developing various sensing and electronic devices.

Acknowledgements

This work was supported by the SUTD-MIT International Design Center (IDG11300101) and the TL@SUTD Seed Grant (IGDS S14 02011) awarded to Y.A.

References

1 S. Iijima, *Nature*, 1991, **354**, 56–58.
2 T. Ebbesen, H. Lezec, H. Hiura, J. Bennett, H. Ghaemi and T. Thio, *Nature*, 1996, **382**, 54–56.
3 R. S. Ruoff and D. C. Lorents, *Carbon*, 1995, **33**, 925–930.
4 J.-M. B. J.-P. Salvetat, N. H. Thomson, A. J. Kulik, L. Forro, W. Benoit and L. Zuppiroli, *Appl. Phys. A*, 1999, **69**, 255–260.
5 B. I. Yakobson and P. Avouris, in *Carbon nanotubes*, Springer, 2001, pp. 287–327.
6 M. F. De Volder, S. H. Tawfick, R. H. Baughman and A. J. Hart, *Science*, 2013, **339**, 535–539.
7 P. Li, N. Lei, D. A. Sheadel, J. Xu and W. Xue, *Sens. Actuators, A*, 2012, **166**, 870–877.
8 P. Li, C. M. Martin, K. K. Yeung and W. Xue, *Biosensors*, 2011, **1**, 23–35.
9 E. Snow, F. Perkins, E. Houser, S. Badescu and T. Reinecke, *Science*, 2005, **307**, 1942–1945.
10 P. Stokes, E. Silbar, Y. M. Zayas and S. I. Khondaker, *Appl. Phys. Lett.*, 2009, **94**, 113104.
11 Y. Duan, J. L. Juhala, B. W. Griffith and W. Xue, *J. Nanopart. Res.*, 2013, **15**, 1–7.
12 H. Lin, L. Li, J. Ren, Z. Cai, L. Qiu, Z. Yang and H. Peng, *Sci. Rep.*, 2013, **3**, 1–6.
13 T. Chen, H. Peng, M. Durstock and L. Dai, *Sci. Rep.*, 2014, **4**, 1–7.
14 C. Papadopoulos and B. Omrane, *Adv. Mater.*, 2008, **20**, 1344–1347.
15 H. Park, A. Afzali, S.-J. Han, G. S. Tulevski, A. D. Franklin, J. Tersoff, J. B. Hannon and W. Haensch, *Nat. Nanotechnol.*, 2012, **7**, 787–791.
16 B.-S. Kim, S. W. Lee, H. Yoon, M. S. Strano, Y. Shao-Horn and P. T. Hammond, *Chem. Mater.*, 2010, **22**, 4791–4797.
17 M. C. LeMieux, M. Roberts, S. Barman, Y. W. Jin, J. M. Kim and Z. Bao, *Science*, 2008, **321**, 101–104.
18 M. Lu, M.-W. Jang, G. Haugstad, S. A. Campbell and T. Cui, *Appl. Phys. Lett.*, 2009, **94**, 261903.
19 D. J. Collins, T. Alan and A. Neild, *Lab Chip*, 2014, **14**, 1595–1603.
20 Y. Ai, C. K. Sanders and B. L. Marrone, *Anal. Chem.*, 2013, **85**, 9126–9134.
21 J. Shi, H. Huang, Z. Stratton, Y. Huang and T. J. Huang, *Lab Chip*, 2009, **9**, 3354–3359.
22 X. Ding, S. C. Lin, M. I. Lapsley, S. Li, X. Guo, C. Y. Chan, I. K. Chiang, L. Wang, J. P. McCoy and T. J. Huang, *Lab Chip*, 2012, **12**, 4228–4231.
23 P. Li, Z. Mao, Z. Peng, L. Zhou, Y. Chen, P.-H. Huang, C. I. Truica, J. J. Drabick, W. S. El-Deiry and M. Dao, *Proc. Natl. Acad. Sci. U. S. A.*, 2015, **112**, 4970–4975.
24 X. Ding, Z. Peng, S.-C. S. Lin, M. Geri, S. Li, P. Li, Y. Chen, M. Dao, S. Suresh and T. J. Huang, *Proc. Natl. Acad. Sci. U. S. A.*, 2014, **111**, 12992–12997.
25 X. Ding, J. Shi, S.-C. S. Lin, S. Yazdi, B. Kiraly and T. J. Huang, *Lab Chip*, 2012, **12**, 2491–2497.
26 J. Shi, D. Ahmed, X. Mao, S.-C. S. Lin, A. Lawit and T. J. Huang, *Lab Chip*, 2009, **9**, 2890–2895.
27 S. Li, F. Guo, Y. Chen, X. Ding, P. Li, L. Wang, C. E. Cameron and T. J. Huang, *Anal. Chem.*, 2014, **86**, 9853–9859.
28 F. Guo, P. Li, J. B. French, Z. Mao, H. Zhao, S. Li, N. Nama, J. R. Fick, S. J. Benkovic and T. J. Huang, *Proc. Natl. Acad. Sci. U. S. A.*, 2015, **112**, 43–48.
29 Y. Chen, X. Ding, S.-C. Steven Lin, S. Yang, P.-H. Huang, N. Nama, Y. Zhao, A. A. Nawaz, F. Guo and W. Wang, *ACS Nano*, 2013, **7**, 3306–3314.
30 Q. Zeng, L. Li, H. L. Ma, J. Xu, Y. Fan and H. Wang, *Appl. Phys. Lett.*, 2013, **102**, 213106.
31 C. J. Strobl, C. Schäflein, U. Beierlein, J. Ebbecke and A. Wixforth, *Appl. Phys. Lett.*, 2004, **85**, 1427.
32 J. Guo, Y. Kang and Y. Ai, *J. Colloid Interface Sci.*, 2015, **455**, 203–211.
33 L. Gor'Kov, *Sov. Phys. –Dokl.*, 1962, **6**, 773.
34 K. Yosioka and Y. Kawasima, *Acta Acust. Acust.*, 1955, **5**, 167–173.
35 H. A. Pohl, *J. Appl. Phys.*, 1951, **22**, 869.
36 H. A. Pohl, *J. Appl. Phys.*, 1958, **29**, 1182–1188.
37 S. B. Asokan, L. Jawerth, R. L. Carroll, R. Cheney, S. Washburn and R. Superfine, *Nano Lett.*, 2003, **3**, 431–437.
38 M. Dimaki and P. Bøggild, *Nanotechnology*, 2004, **15**, 1095.
39 J. J. Boote and S. D. Evans, *Nanotechnology*, 2005, **16**, 1500–1505.

40 S. Ghosh, A. Sood and N. Kumar, *Science*, 2003, **299**, 1042–1044.
41 L. Cai, L. Song, P. Luan, Q. Zhang, N. Zhang, Q. Gao, D. Zhao, X. Zhang, M. Tu and F. Yang, *Sci. Rep.*, 2013, **3**, 1–8.
42 T. Yamada, Y. Hayamizu, Y. Yamamoto, Y. Yomogida, A. Izadi-Najafabadi, D. N. Futaba and K. Hata, *Nat. Nanotechnol.*, 2011, **6**, 296–301.
43 D. J. Lipomi, M. Vosgueritchian, B. C. Tee, S. L. Hellstrom, J. A. Lee, C. H. Fox and Z. Bao, *Nat. Nanotechnol.*, 2011, **6**, 788–792.
44 H. Morgan and N. G. Green, *J. Electrost.*, 1997, **42**, 279–293.
45 K. D. Hermanson, S. O. Lumsdon, J. P. Williams, E. W. Kaler and O. D. Velev, *Science*, 2001, **294**, 1082–1086.
46 A. Monica, S. Papadakis, R. Osiander and M. Paranjape, *Nanotechnology*, 2008, **19**, 085303.